THE JOURNAL OF PHYSICAL CHEMISTRY C

ARTICLE

pubs.acs.org/JPCC

NO_x Interactions with Dispersed BaO: Adsorption Kinetics, Chemisorbed Species, and Effects of Oxidation Catalyst Sites

Brian M. Weiss,[†] Kyle B. Caldwell,[†] and Enrique Iglesia*[,†,‡]

[†]Department of Chemical Engineering, University of California, Berkeley, California 94720, United States

[‡]E. O. Lawrence Berkeley National Laboratory, Berkeley, California 94720, United States

Supporting Information

ABSTRACT: Infrared spectra and nitrate and nitrite formation rate data free of transport artifacts provide rigorous evidence for the identity of the adsorbed species and the elementary steps required for adsorption of NO, NO_2, and CO_2 on BaO/Al_2O_3 with and without Pt clusters that act as oxidation catalysts. NO/NO_2 adsorption occurs via initial formation of nitrites and their subsequent oxidation to nitrates on samples presaturated with carbonates by exposure to CO_2. Nitrites form much faster than nitrates at low NO_2 pressures via displacement of carbonates and vicinal coadsorption of NO and NO_2 molecules. As a result, the dynamics of nitrite formation and of their subsequent oxidation can be independently measured during exposure to NO/NO_2 mixtures over a broad temperature range (453−673 K). Nitrites form rapidly upon exposure to NO_x, but the presence of CO_2 limits equilibrium NO_x uptakes because of unfavorable thermodynamics, rendering nitrite formation an impractical strategy for NO_x removal from CO_2-rich combustion effluent streams. Nitrate thermodynamics is much more favorable, but the rate of nitrite oxidation to nitrates is limited by slow homogeneous NO_2 dimerization to N_2O_4, which acts as the oxidant in nitrite conversion to nitrates on Pt-free Ba/Al_2O_3. This mechanism is consistent with nitrate formation rates that are second-order in NO_2 pressure and essentially independent of NO pressure, sample temperature, and residual coverages of unreacted nitrites. Pt clusters present in close proximity to (but not atomic contact with) nitrite-saturated BaO domains provide a catalytic route for the formation of the N_2O_4 oxidant required to convert nitrites to stable nitrates and for the effective removal of NO_x from CO_2-containing streams. Nitrate formation rates on $BaO/Pt/Al_2O_3$ are proportional to NO_2 pressures, inhibited by NO and proportional to the residual coverage of unreacted nitrites, consistent with rates limited by reactions between N_2O_4 molecules, in equilibrium with NO_2 in steps mediated by Pt surfaces, and nitrites. These detailed kinetic and spectroscopic studies provide mechanistic details previously unavailable about the bifunctional character of NO_2 reactions that form stable nitrates on BaO domains and about the essential role of oxidant formation on metal clusters in rendering such adsorption strategies practical for the removal of NO_x from CO_2-rich streams.

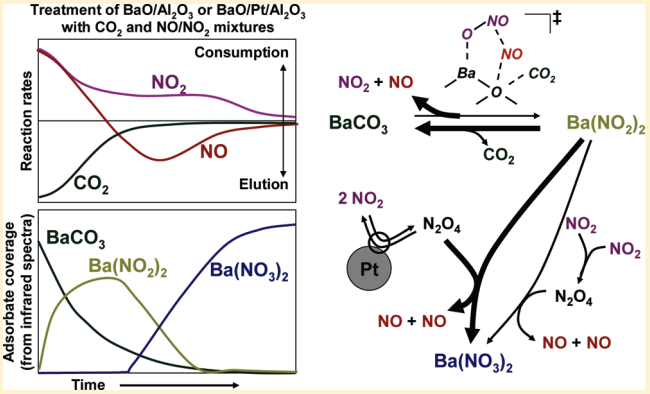

1. INTRODUCTION

BaO adsorbents, together with transition metal catalysts, can be used to trap smog-causing NO from combustion effluent streams that lack CO or residual hydrocarbons as reductants.[1−3] Transition metals catalyze NO oxidation to NO_2, a molecule that readily adsorbs on many porous solids,[4,5] but which also inhibits NO oxidation by titrating active sites on catalytic surfaces with oxygen atoms.[6−8] As a result, NO_2 adsorption rates on BaO or $BaCO_3$ strongly influence the effectiveness of the catalysts required to convert NO to NO_2 as part of lean de-NO_x removal strategies.[7,8]

Infrared and X-ray photoelectron spectroscopic studies suggest that NO_2 initially adsorbs on BaO-containing solids as nitrites with either sequential[5,9−16] or concurrent[12−17] formation of nitrates. Nitrate formation can involve peroxides (BaO_2)[5,18,19] or direct interactions of NO_2[5,8−23] or NO/O_2[15,16,20] with BaO surfaces or with preformed nitrites. Nitrite and nitrate formation on BaO may also be mediated by intermediates formed on proximate metal clusters.[15,16,20−22] The elementary steps for NO_x adsorption processes and the transport pathways between Pt and BaO sites remain unclear and controversial, at least in part, because previous studies have been conducted at conditions leading to complete NO_2 conversion, which preclude unequivocal interpretations of adsorption and reaction rates.

Here, we report infrared spectra and kinetic data under conditions of strict kinetic control to probe the nature of the

Received: November 5, 2010
Revised: February 15, 2011
Published: March 23, 2011

adsorbed species, reactions, and elementary steps involved in the competitive adsorption of CO_2 and NO_x on BaO/Al_2O_3 and $BaO/Pt/Al_2O_3$. The formation of nitrates is slow at low NO_2 pressures (<9 Pa), and such conditions allow measurements of nitrite formation rates during contact with NO/NO_2 mixtures without concurrent nitrate formation. Consequently, we have prepared well-defined systems to study the rates of nitrite formation, the thermodynamics of nitrite−carbonate interconversion, and the dynamics of nitrite conversion to nitrates in the absence and presence of Pt catalysts. Our results indicate that the relative stabilities of nitrite and carbonate lead to low nitrite coverages in the presence of CO_2, making nitrites ineffective as adsorbed species in NO_x trapping strategies. The sequential formation of more stable nitrates allows larger NO_x uptakes, but nitrate formation rates in metal-free adsorbents are limited by slow NO_2 dimerization steps that form species required to oxidize nitrite. Intermediates formed on Pt sites present as coimpregnated mixtures with nitrite binding sites provide alternate and much faster nitrate formation pathways that allow for more efficient use of NO_2 adsorbents.

2. EXPERIMENTAL METHODS

2.1. BaO/Al_2O_3 and $BaO/Pt/Al_2O_3$ Synthesis. Materials were prepared by similar methods as in previous studies.[15,23] γ-Al_2O_3 (Sasol, SBa-200, 180 $m^2\ g^{-1}$) was heated to 1023 K at 0.06 K s^{-1} in flowing dry air (Praxair, extra dry; 1 $cm^3\ g\ s^{-1}$) and held at 1023 K for 4 h. Pt/Al_2O_3 (2.1 wt % Pt) was prepared by methods described previously[7] to achieve a material with 76% of Pt atoms exposed at cluster surfaces, which corresponds to Pt clusters with a mean size of 1.2 nm and a dispersion of 0.0059 Pt clusters per nm^2 assuming hemispherical geometries and a density equal to the bulk value (22 g cm^{-3} [24]). Either γ-Al_2O_3 or this Pt/Al_2O_3 was combined with an aqueous solution [0.45 cm^3 (g $Al_2O_3)^{-1}$] of $Ba(O_2C_2H_3)_2$ (Sigma-Aldrich, 99.995%) to achieve loadings of 3.0 BaO nm^{-2} (15 wt % $BaCO_3$). Impregnated samples were held at 383 K for 6 h in ambient air and then heated to 823 K at 0.06 K s^{-1} in flowing dry air (1 $cm^3\ g^{-1}\ s^{-1}$) and held for 4 h. A portion of the BaO/Al_2O_3 adsorbents was pulverized in 1:3 ratios with either 2.1 wt % Pt/Al_2O_3 (0.76 Pt dispersion) or SiO_2 [Selecto, treated at 1123 K in flowing dry air (1 $cm^3\ g^{-1}\ s^{-1}$) for 4 h].

2.2. CO_2 and NO_x Adsorption Measurements. Adsorption thermodynamics and kinetics were measured on self-supported wafers (2−6 mg cm^{-2}, pressurized at 100 MPa) in an infrared cell described previously[25] and on pellets (0.02−0.1 mm diameter; formed by pressurization of powders at 100 MPa) supported on a quart wool plug within a quartz tubular reactor (4 mm diameter). Temperatures (423−673 K) were held constant using resistive heating and an electronic controller (Watlow 96 series). Mass flow controllers (Porter Instruments) and switching valves (Valco Instruments Co.) were automated using Labview software (National Instruments). Reactant gases (0.1% NO_2/He, 2% NO/He, 10% CO_2/He, H_2) and a He balance (Praxair; 99.999% purity) were metered to achieve 10^{-3}−10^{-1} kPa of NO_2, 10^{-2}−10^{0} kPa of NO, 10^{-1}−10^{1} kPa of CO_2, 3 kPa of H_2, and 10^2 kPa of total pressure. Reactor inlet and outlet concentrations of NO, NO_2, and CO_2 were measured by an infrared gas analyzer (MKS 2030, 2 cm cell, 2 cm path length), while adsorbates were detected by a Fourier-transform infrared spectrometer (Thermo-Nicolet 8700; transmission mode). BaO/Al_2O_3 adsorbents were discarded after their saturation with nitrate, but adsorption sites on nitrate-saturated $BaO/Pt/Al_2O_3$ were regenerated by treatment with 3 kPa of H_2 (473−573 K) for 0.5 h.

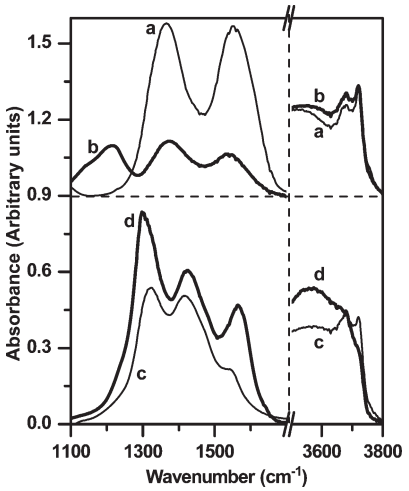

Figure 1. Infrared spectra of BaO/Al_2O_3 (3.0 BaO nm^{-2}) samples at 573 K treated with (a) 1 kPa of CO_2 for 1 h and then with a NO_2/NO mixture that contained either (b) 4.0 Pa of NO_2, 120 Pa of NO, (c) 30 Pa of NO_2, 120 Pa of NO, or (d) 100 Pa of NO_2. The NO/NO_2 treatments were performed for 1 h on each sample. Spectra were normalized so that the carbonate band area (1250−1650 cm^{-1}) during the CO_2 treatment was the same on each sample.

Adsorbate coverages were determined from infrared spectra by methods presented in the Appendix. NO and NO_2 conversions were kept below 15% for kinetic measurements by adjusting molar flow rates [9−400 mol (mol BaO)$^{-1}$ s^{-1}]. Adsorption rates were normalized by the available surface area, the pore volume, or the number of accessible nitrite binding sites (denoted BaO_n). Rates of the fastest process, nitrite formation on BaO/Al_2O_3 (5 Pa of NO_2, 75 Pa of NO, 503 K), were similar on 80 μm pellets of BaO/Al_2O_3 [5.3×10^{-3} mol (mol $BaO_n)^{-1}$ s^{-1}] and on 20 μm pellets [6.1×10^{-3} mol (mol $BaO_n)^{-1}$ s^{-1}] containing 1:3 mixtures of BaO/Al_2O_3 and SiO_2, confirming the absence of mass transfer artifacts.[26]

3. RESULTS AND DISCUSSION

3.1. Adsorbed Species and Reactions Involved in CO_2 and NO_x Adsorption on BaO/Al_2O_3 and $BaO/Pt/Al_2O_3$. In this section, we provide evidence for the identity of the adsorbed species and for the pathways involved in CO_2 and NO_x adsorption on BaO/Al_2O_3 and $BaO/Pt/Al_2O_3$. The infrared spectra in Figures 1 and 2 show the main features of all infrared-active adsorbed species detected in this study. These spectra resemble those in previous reports, in which observed bands were assigned to carbonate[27−29] (Figure 1a, 2a; 1250−1650 cm^{-1}), nitrite[9,15,30,31] (Figure 2d; 1100−1250 cm^{-1}), and nitrate[9,15,31,32] (Figure 1c, 2e; 1275−1500 cm^{-1}) on BaO structures. We note that the two antisymmetric carbonate stretches show different vibrational frequencies (Figures 1a, 2a), indicating that carbonates were formed only at BaO surfaces.[27] Our infrared spectra (Figures 1d, 2b,f) also showed bands characteristic of nitrates on BaO and on γ-Al_2O_3[9,33] (1250−1350, 1500−1650 cm^{-1}). Unperturbed (3650−3750 cm^{-1}) and perturbed (3400−3600 cm^{-1}) hydroxyl groups[34] were also present on γ-Al_2O_3. The respective frequencies of the carbonate, nitrite, and nitrate bands were similar on BaO/Al_2O_3 (Figure 1) and $BaO/Pt/Al_2O_3$ (Figure 2)

dx.doi.org/10.1021/jp110604j |J. Phys. Chem. C 2011, 115, 6561–6570

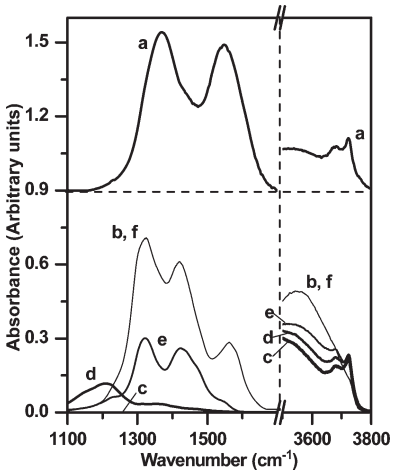

Figure 2. Infrared spectra of $BaO/Pt/Al_2O_3$ (3.0 BaO nm^{-2}) at 503 K treated with (a) 1 kPa of CO_2 for 15 ks and treated with (b) 100 Pa of NO_2 for 4 ks and then treated with (c) 3 kPa of H_2 for 2 ks. After H_2 treatment, the sample was treated with a mixture of 5.2 Pa of NO_2 and 75 Pa of NO (e) for 0.2 ks and (f) for 3 ks; and finally treated with (g) 100 Pa of NO_2 for 4 ks.

at all conditions used in this study, indicating that binding sites and bound species are not influenced by the presence of Pt.

The interactions of CO_2 and NO/NO_2 mixtures with BaO/Al_2O_3 were examined by concurrent measurements of adsorbate coverages and NO_x consumption and CO_2 evolution rates. Treatment of BaO/Al_2O_3 at 573 K with 1 kPa of CO_2 for 1 h led to surface carbonates (0.7 $BaCO_3$ nm^{-2}; Figure 3a, 0 ks). Subsequent treatment of this sample with a mixture of 30 Pa of NO_2 and 120 Pa of NO at 573 K caused nitrite coverages to increase and carbonate coverages to simultaneously decrease (Figure 3a, 0−0.5 ks), consistent with the displacement of carbonates by nitrites. The formation of nitrites occurred only when both NO and NO_2 were introduced, consistent with the equimolar consumption of NO and NO_2 (Figure 3b, 0−0.5 ks); CO_2 was concurrently evolved as nitrites formed, and the rate of CO_2 desorption was the same as the NO_2 (and NO) consumption rate (Figure 3b, 0−0.5 ks). Treatment of BaO/Al_2O_3 with 30 Pa of NO_2 and 120 Pa of NO eventually led to the formation of nitrates on BaO (Figure 3a, 1−12 ks), to the ultimate disappearance of nitrites and of all carbonate species, and to the consumption of NO_2 and the evolution of NO (Figure 3b, 1−12 ks). The amount of NO_2 consumed per NO evolved was 2.9 over the time period shown in Figure 3, consistent with previous reports on BaO/Al_2O_3 (3.0 NO_2 consumed per NO evolved[4,35]). Nitrate formation was also observed on γ-Al_2O_3 (Figure 3a, 3−10 ks) and occurred concurrently with a decrease in the intensity of bands assigned to unperturbed OH groups on γ-Al_2O_3 (Figure 3a, 1−10 ks) and an increase in the intensity of a broad band at lower frequencies assigned to perturbed OH groups (Figure 1c,d). No other adsorbed species were evident in the infrared spectra (1100−1700 cm^{-1}) of BaO/Al_2O_3 during NO/NO_2 treatments (Supporting Information, Figure S1, with additional discussion in the Appendix).

We also investigated the interactions of NO/NO_2 mixtures with $BaO/Pt/Al_2O_3$ samples to determine any effects of Pt on adsorption reactions. Nitrites formed initially during contact of $BaO/Pt/Al_2O_3$ at 503 K with a mixture of 75 Pa of NO and 5.2 Pa of NO_2 (Figure 4, 0.0−0.2 ks) and occupied a large

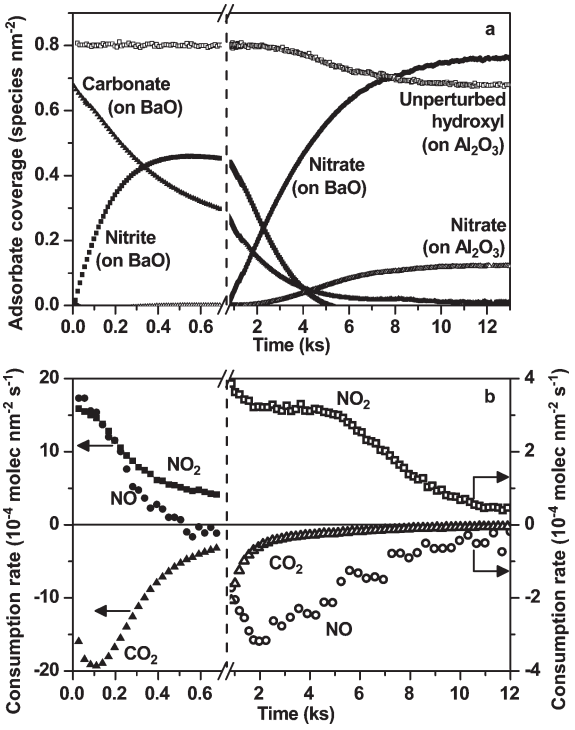

Figure 3. (a) Adsorbate coverages and (b) NO, NO_2, and CO_2 consumption rates as a function of time on BaO/Al_2O_3 (3.0 BaO nm^{-2}) at 573 K treated with 150 Pa of NO and 30 Pa of NO_2 (17×10^{-4} NO_2 nm^{-2} s^{-1}). Sample was treated at 573 K with 1 kPa of CO_2 for 1 h and then with flowing He for 200 s before introduction of the NO/NO_2 mixture.

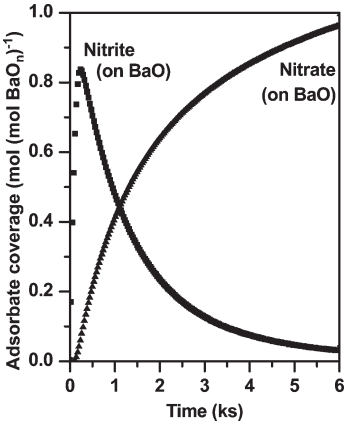

Figure 4. Adsorbate coverages on $BaO/Pt/Al_2O_3$ (3.0 BaO nm^{-2}) at 503 K as a function of contact time with a mixture of 75 Pa of NO and 5.2 Pa of NO_2. Sample treated at 503 K with 100 Pa of NO_2 for 0.5 h and then with 3 kPa of H_2 for 0.5 h before introduction of NO/NO_2 mixtures. Carbonate on BaO and nitrate on Al_2O_3 were not detected during the treatment at 75 Pa of NO, 5.2 Pa of NO_2, 503 K.

fraction of the accessible binding sites. These nitrite species were replaced by nitrates in slower sequential reactions (Figure 4, 0.2−6.0 ks). Carbonates were present initially on $BaO/Pt/Al_2O_3$ samples treated with 1 kPa of CO_2 (Figure 2a) but were no longer detected after samples were treated at 503 K with 100 Pa of NO_2 for 4 ks and then with 3 kPa of H_2 for 2 ks (Figure 2c). Nitrates were also fully removed by treatment with 3 kPa of H_2 at 453−553 K for 2 ks (Figure 2c).

dx.doi.org/10.1021/jp110604j |J. Phys. Chem. C 2011, 115, 6561–6570

Scheme 1. CO_2 and NO_x Adsorption Reactions on BaO/Al_2O_3 and $BaO/Pt/Al_2O_3$

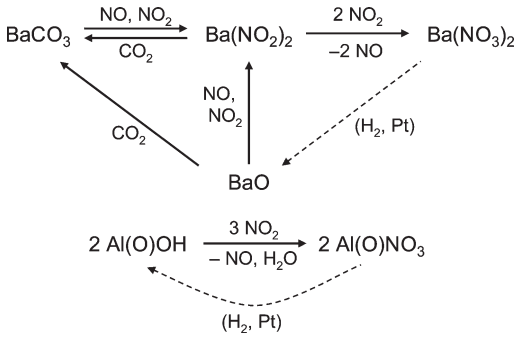

The reactions in Scheme 1, which are not intended to describe elementary processes, account for the observed interconversions among the most abundant adsorbed species present on BaO/Al_2O_3 and $BaO/Pt/Al_2O_3$, as shown by the data in Figures 3 and 4. Scheme 1 includes reactions between carbonate ($BaCO_3$) and NO/NO_2 to form CO_2 and nitrite [$Ba(NO_2)_2$] and between NO_2 and nitrite to form NO and nitrate [$Ba(NO_3)_2$]. The sequential replacement of surface carbonates by nitrites and ultimately by nitrates, taken together with the minor changes in the nitrite and nitrate infrared features during NO/NO_2 treatments (Supporting Information, Figure S1), indicates that infrared-active species were predominantly present at BaO surfaces. The conversion of hydroxyls on γ-Al_2O_3 [Al(O)OH] to nitrates [$Al(O)NO_3$] is also shown in Scheme 1 and is consistent with the consumption of three NO_2 molecules per NO released. We note that the slow formation of nitrates on both BaO and Al_2O_3 sites (Figures 3 and 4) allows measurements of nitrite formation rates (discussed next) before significant amounts of nitrates form and also allows subsequent measurements of nitrate formation rates on surfaces initially treated to form nitrites at saturation coverages (discussed in sections 3.4 and 3.5).

3.2. Nitrite Formation Rates on BaO/Al_2O_3. Nitrite formation rates were measured by holding BaO/Al_2O_3 at constant temperature (423−673 K) and treating each sample with 1 kPa of CO_2 for 1 h and then in flowing He [400 mol He $(\text{mol BaO}_n)^{-1}$ s^{-1}; 200 s] before introducing mixtures containing NO (0−100 Pa) and NO_2 (0−11 Pa). Nitrite formation rates were measured from CO_2 evolution rates, which were equal to nitrite formation rates (Figure 5) but were measured more accurately than differences in NO and NO_2 concentrations in the inlet and outlet streams. All rates were normalized by the number of nitrite binding sites (L_n) determined from the NO_2 uptake on BaO/Al_2O_3 treated with a mixture of 8 Pa of NO_2 and 560 Pa of NO (reported in the Supporting Information, Figure S2). We note that the steady-state coverage of adsorbed species measured by infrared spectroscopy varied weakly when the NO and NO_2 pressures were varied between 20 and 500 Pa of NO and 1−8 of Pa NO_2 (Supporting Information, Figure S3), but the NO_2 uptake decreased modestly with increasing treatment temperature (Supporting Information, Figure S2). These results suggest that all reactive BaO structures became saturated with nitrite when treated with a mixture of 8 Pa of NO_2 and 560 Pa of NO, but some BaO structures were converted to unreactive ones with increasing treatment temperature. As a result, a different value of L_n was used to normalize rates at each temperature, using the uptake values measured at that temperature (Supporting Information, Figure S2).

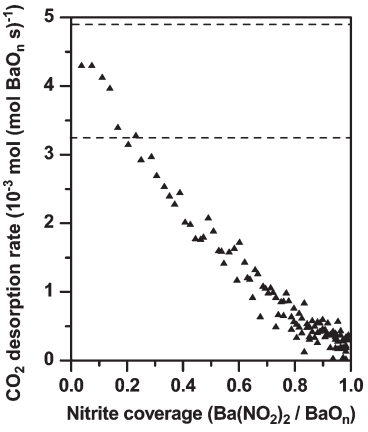

Figure 5. Nitrite formation rates normalized by BaO_n and plotted as a function of nitrite coverage on BaO/Al_2O_3 (3.0 BaO nm^{-2}) at 523 K treated with 6.0 Pa of NO_2 and 53 Pa of NO. Sample was treated at 523 K with 1 kPa of CO_2 for 1 h and then in flowing He for 200 s before introduction of NO/NO_2 mixtures. Dashed lines give the detected range for initial NO_2 adsorption rate [$4.1 \pm 0.8 \times 10^{-3}$ mol $(\text{mol BaO}_n)^{-1}$ s^{-1}].

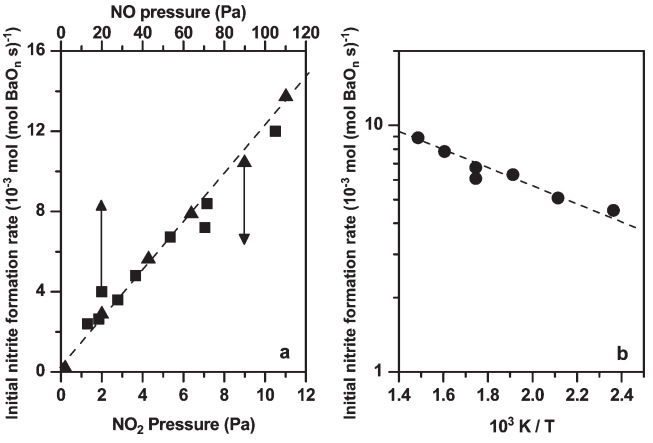

Figure 6. Nitrite formation rates extrapolated to the initial saturation carbonate coverage and normalized by BaO_n on BaO/Al_2O_3 (3.0 BaO nm^{-2}). Rates (a) at 573 K versus (■) NO (at 6.0 Pa of NO_2) or (▲) NO_2 (at 55 Pa of NO) pressures; (b) rates at 6.0 Pa of NO_2 and 55 Pa of NO as a function of temperature plotted in an Arrhenius format. Samples were treated at 573 K with 1 kPa of CO_2 for 1 h and then in flowing He for 300 s before introduction of NO/NO_2 mixtures.

Nitrite formation rates decreased almost linearly with increasing nitrite coverage as carbonates converted to nitrites with increasing contact time (Figure 5; 6 Pa of NO, 55 Pa of NO, 523 K). Nitrite formation rates were proportional to both NO (0−80 Pa) and NO_2 (0−11 Pa) pressures (Figure 6a) during initial contact of BaO/Al_2O_3 with NO/NO_2 mixtures; these rates were weakly influenced by temperature (423−673 K; Figure 6b), indicative of a very small apparent activation energy for nitrite formation (5 ± 2 kJ mol^{-1}). Previous studies of NO_2 adsorption rates on carbonate-saturated BaO/Al_2O_3 (NO_2 formed by NO oxidation on Pt/Al_2O_3 mixed with BaO/Al_2O_3) also showed that nitrite formation rates on carbonate-saturated surfaces increased linearly with NO_2 pressure and were not influenced by CO_2

dx.doi.org/10.1021/jp110604j |J. Phys. Chem. C 2011, 115, 6561–6570

pressure (0.0−0.5 kPa),[7] but kinetic dependences on NO pressures and temperatures were not reported.

The measured nitrite formation rates on BaO/Al_2O_3 surfaces initially saturated with carbonate species ($r_{c\text{-}n}$) are accurately described by the equation:

$$r_{c-n} = k_{c-n}[NO][NO_2](L_n - [Ba(NO_2)_2])(1-\eta) \quad (1)$$

in which L_n is the number of nitrite binding sites, η (eq 2) accounts for the approach to equilibrium for the nitrite−carbonate interconversion (eq 3)

$$\eta = \frac{[Ba(NO_2)_2]}{K_{c-n}[BaCO_3]\psi} \quad (2)$$

$$BaCO_3 + NO + NO_2 \rightleftarrows Ba(NO_2)_2 + CO_2 \quad (3)$$

and ψ describes the thermodynamic driving force for this interconversion

$$\psi = \frac{[NO_2][NO]}{[CO_2]} \quad (4)$$

The values of the equilibrium constant, $K_{c\text{-}n}$, for the nitrite−carbonate interconversion at BaO surfaces are reported and discussed in section 3.3. The measured rate constant for nitrite formation, $k_{c\text{-}n}$ [2.1×10^{-5} mol (mol BaO_n)$^{-1}$ s^{-1} Pa^{-2} at 573 K], is similar to the NO_2 adsorption rate constant previously reported [1.4×10^{-5} mol (mol BaO_n)$^{-1}$ s^{-1} Pa^{-2}][7] on mixtures of Pt/Al_2O_3 and BaO/Al_2O_3 treated with 170 Pa of NO and 500 Pa of O_2 at 573 K. The nitrite formation rate constant from this previous study[7] was derived from reported values of the NO consumption rate [0.65 mol NO (mol Pt_s) s^{-1}], the Pt_s/BaO_n ratio (5.6×10^{-3}), and the NO_2 pressure (0.8 Pa; determined from the NO oxidation kinetics). Our results therefore agree with previous measurements[7] of nitrite formation rates.

The measured kinetic responses described by eq 1 indicate that kinetically relevant nitrite formation steps involve species containing NO and NO_2. The linear decrease in rates with increasing nitrite coverage (eq 1) indicates that kinetically relevant nitrite formation steps occur on accessible binding sites that are not occupied by nitrites. The absence of inhibition of initial nitrite formation rates by CO_2[7] suggests that the formation of an unoccupied site via equilibrium CO_2 adsorption−desorption is not a prerequisite for NO/NO_2 adsorption, which must instead occur in a concerted manner with CO_2 desorption. The small apparent activation energy for nitrite formation (5 ± 2 kJ mol^{-1}) suggests that the reactants and transition state involved in nitrite formation have similar energies. This appears to reflect the concerted nature of the NO/NO_2 adsorption and CO_2 desorption steps, because sequential desorption of CO_2 before NO/NO_2 adsorption would involve an activation barrier commensurate with the CO_2 adsorption heat [230 or 272 kJ mol^{-1} on BaO(100)[36] or bulk $BaCO_3$,[24] respectively].

The individual presence of NO or NO_2 (Figure 6a) did not lead to NO_x adsorption on carbonate-saturated BaO adsorbents. DFT-derived binding energies for vicinal NO and NO_2 adsorbed on BaO(100) are larger (by 80 kJ mol^{-1})[36] than for noninteracting NO and NO_2 adsorbates, suggesting that stabilization by coadsorbed NO_x is required to bind NO or NO_2. Yet, even vicinal adsorption of NO and NO_2 as nitrites leads to species that are slightly more stable than adsorbed CO_2 (by 70 kJ mol^{-1} on bulk BaO[24]), which is present in very large excess in automotive exhaust ($CO_2/NO_x > 10^3$).

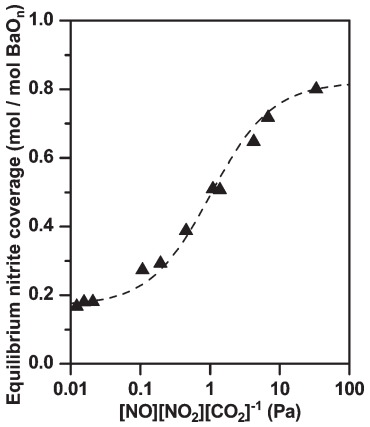

Figure 7. Equilibrium nitrite coverages determined from NO_2 uptakes at 573 K on BaO/Al_2O_3 (3.0 BaO nm^{-2}) versus ψ (=$[NO][NO_2][CO_2]^{-1}$). Samples were previously treated at 573 K with 1 kPa of CO_2 for 1 h. BaO_n determined from the NO_2 uptake on BaO/Al_2O_3 at 573 K treated with 120 Pa of NO and 6 Pa of NO_2 until the nitrite coverage reached a constant value. The dashed curve shows the prediction of eq 5.

3.3. Thermodynamics of Nitrite and Carbonate Formation on BaO/Al_2O_3. We consider next the thermodynamics of competitive formation of nitrite and carbonate species over a broad concentration range. The rapid formation of nitrites during treatment of BaO/Al_2O_3 with NO/NO_2 mixtures (423−673 K) allowed efficient NO_x trapping as nitrites, but the addition of CO_2 to NO/NO_2 mixtures significantly decreased equilibrium nitrite coverages (Figure 7). Equilibrium nitrite coverages on BaO/Al_2O_3 samples were similar for gas mixtures containing a constant value of ψ ($[NO][NO_2][CO_2]^{-1}$), but different individual NO, NO_2, and CO_2 pressures (Supporting Information, Figure S4), consistent with ψ as the rigorous thermodynamic driving force for nitrite−carbonate interconversion. Equilibrium nitrite coverages decreased strongly with decreasing ψ (Figure 7) over the range of NO (40−460 Pa), NO_2 (2.7−8.0 Pa), and CO_2 (0.1−9 kPa) pressures examined.

Equilibrium nitrite coverages were accurately described by an adsorption isotherm that involves three types of binding sites (eq 5; dashed curve in Figure 7). One site is saturated with nitrite, while another one remains occupied by carbonate over the reported range of ψ values (0.01−30 Pa). The remaining sites, which account for most of the binding sites in these samples, exist at surfaces that reversibly adsorb NO_x and CO_2 according to a Langmuir isotherm with equilibrium constant $K_{c\text{-}n}$ (eq 3):

$$\frac{[Ba(NO_2)_2]}{L_n} = \alpha + \beta\frac{K_{c-n}\psi}{1 + K_{c-n}\psi} \quad (5)$$

α represents the fraction of sites that remain saturated with nitrite for ψ above 10^{-2} Pa, and β represents the fraction of sites with equilibrium constant $K_{c\text{-}n}$. The three-site model (eq 5) represents a simplification of the true system, which likely contains BaO domains with a distribution of sizes and binding properties. Yet, previous computational results showed that the binding energies of isolated carbonates and nitrites have similar

dx.doi.org/10.1021/jp110604j |J. Phys. Chem. C 2011, 115, 6561–6570

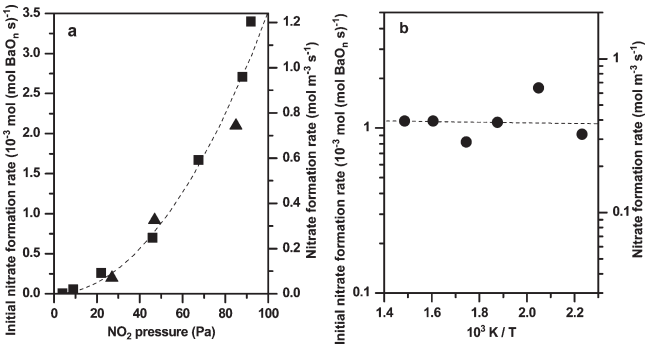

Figure 8. Nitrate formation rates extrapolated to the initial saturated nitrite coverage and normalized by BaO_n (left axis) or pore volume (right axis) during treatment of BaO/Al_2O_3 with NO/NO_2 mixtures. (a) Rates at 573 K (▲) with 110 Pa of NO and (■) without added NO and (b) rates as a function of temperature plotted in an Arrhenius format at 47 Pa of NO_2 without added NO. Samples were previously treated with a mixture of 120 Pa of NO and 4.0 Pa of NO_2 for 1 h at 573 K to reach saturation nitrite coverages. The dashed curve shows the prediction from eq 6.

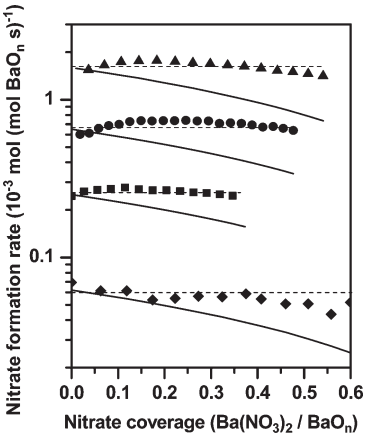

Figure 9. Nitrate formation rates, normalized by BaO_n, on BaO/Al_2O_3 (3.0 BaO nm^{-2}) at 573 K treated with (◆) 10 Pa, (■) 22 Pa, (●) 46 Pa, and (▲) 70 Pa of NO_2. Samples were previously treated with a mixture 120 Pa of NO and 4.0 Pa of NO_2 for 1 h at 573 K to reach saturation nitrite coverage. The solid and dashed curves show the predictions of eqs 6 and 7, respectively, for each data set.

sensitivities to the basicity of the substrate,[36] and these calculations suggest that a single equilibrium constant describes the competitive binding of carbonate and nitrite on sites with different intrinsic basicities, in contrast with our observed results. The slight deviations that we observe from uniform site models may reflect repulsive interactions among adsorbed species, which can also influence their collective binding energies.

The parameters required to describe the data in Figure 7 and eq 5 indicate that a small fraction of sites [$\alpha = 0.17 \pm 0.02$ mol (mol BaO_n)$^{-1}$] has a stronger affinity for nitrite than carbonate at values of ψ as low as 10^{-2} Pa. A majority of binding sites [$\beta = 0.65 \pm 0.04$ mol (mol BaO_n)$^{-1}$] behave as a uniform ensemble with thermodynamic properties for the nitrite−carbonate interconversion that can be described by an equilibrium constant ($K_{c\text{-}n} = 0.97 \pm 0.25$ Pa^{-1}) that resembles estimates ($K_{c\text{-}n} = 0.35$ Pa^{-1} at 573 K) from DFT-derived nitrite (360 kJ mol^{-1}) and carbonate (230 kJ mol^{-1}) binding energies on BaO(100)[36] and entropy changes for the nitrite−carbonate given by differences in the translational entropies of NO, NO_2, and CO_2 as gaseous molecules (−140 J mol^{-1} K^{-1}[37]). Such low values of $K_{c\text{-}n}$ cause carbonate to be preferred over nitrite in gas mixtures with values of ψ typically produced by combustion engines ($\psi < 10^{-2}$ Pa^{-1}, ~10^4 Pa of CO_2, ~20 Pa of NO_x). The conversion of carbonate to nitrate is much more exothermic (−180 to −240 kJ mol^{-1}[24,36]) than to nitrite (−70 to −130 kJ mol^{-1}[24,36]), and the equilibrium constants for carbonate-to-nitrate conversion are therefore much larger (10^1−10^6 Pa^{-1} at 573 K). As a result, the conversion of nitrites to nitrates becomes an essential requirement for the efficient removal of NO_x from CO_2-containing combustion effluent streams.

3.4. Nitrate Formation Rates on BaO/Al_2O_3. Nitrate formation rates were measured on BaO/Al_2O_3 samples (without Pt) previously treated with NO/NO_2 mixtures (120/4.0 Pa) for 1 h at each reaction temperature (453−673 K) until the nitrite coverage reached a constant value (~1 h on-stream). Initial nitrate formation rates were unaffected by NO pressure and temperature (Figure 8) but increased strongly with increasing NO_2 pressure with a dependence that was accurately described as proportional to $(NO_2)^2$ (Figure 8a, dashed curve). Nitrate formation rates from pre-existing nitrites ($r_{n\text{-}N}$) remained essentially constant, even after significant amounts of nitrite were converted to nitrate (Figure 9). These nitrate formation rates were accurately described by the rate equation (Figure 9, dashed curves)

$$r_{n-N} = k_{n-N}[NO_2]^2[NO]^0[Ba(NO_x)_2]^0 = k_{n-N}[NO_2]^2 \quad (6)$$

but not by the alternate equation expected if rates were proportional to the remaining amounts of nitrite in the sample (Figure 9, solid curves)

$$r_{n-N} = k'_{n-N}[NO_2]^2[NO]^0[Ba(NO_x)_2]^1 \quad (7)$$

The temperature dependence of the measured rate constant ($k_{n\text{-}N}$ in eq 6) gave essentially no detectable activation energy (0 ± 5 kJ mol^{-1}). We note that nitrite formation rates do not depend on coverage for values of nitrite coverage below 50% (Figure 9). Nitrate formation rates decrease with increasing nitrate coverage at higher nitrate coverages (as observed in Figure 3a). This decrease in rate reflects steps that are much slower than those limiting nitrite formation rates at low coverages; therefore, they are kinetically insignificant during the early stages of nitrite formation.

The functional form of eq 6 indicates that the oxidation of nitrite to nitrate species is mediated by intermediates containing two NO_2 molecules, without detectable involvement of NO. This kinetic dependence suggests the participation of NO_2 dimers (e.g., N_2O_4) whose equilibrium pressures are very low at these conditions (10^{-9}−10^{-4} Pa;[24] 4−100 Pa of NO_2, 453−673 K), thus requiring their formation near BaO binding sites (i.e., within sample pores or intrapellet space). The weak effects of residual nitrite coverages on nitrate formation rates (eq 6) suggest that such rates are limited by steps that do not occur on $Ba(NO_2)_2$ surfaces. These data indicate that NO_2 forms N_2O_4 via homogeneous dimerization pathways within the pore volume and that this step is rendered irreversible and rate-determining by the rapid subsequent reaction of N_2O_4 with nitrites to form nitrates with evolution of NO. NO_2 dimerization

Table 1. Nitrite and Nitrate Formation Rates on BaO/Al_2O_3 and $BaO/Pt/Al_2O_3$[a]

material[b]	formation rate, 10^{-4} mol (mol BaO_n)$^{-1}$ s^{-1}	
	nitrite[c]	nitrate[d]
BaO/Al_2O_3	61	0.10 [e]
mechanically ground BaO/Al_2O_3 + Pt/Al_2O_3 (3: 1 ratio)	49	0.14 [e]
coimpregnated $BaO/Pt/Al_2O_3$	54	6.4 [f]

[a] Rates at 503 K, 5.2 Pa of NO_2, 75 Pa of NO. [b] Loadings of 3.0 BaO nm^{-2}, 0.0059 Pt clusters nm^{-2}. [c] Rates extrapolated to initial saturated carbonate coverage on samples pretreated at 503 K with 1 kPa of CO_2 for 1 h. [d] Rates extrapolated to saturation nitrite coverage. [e] Samples pretreated at 503 K with a mixture of 5.2 Pa of NO_2 and 75 Pa of NO for 1 h. [f] Samples pretreated at 503 K with 100 Pa of NO_2 for 0.5 h and then with 3 kPa of H_2 for 0.5 h.

to form the D_{2h} isomer of N_2O_4 (O_2N-NO_2) occurs in the gas phase without detectable activation barriers.[38] Homogeneous rates (0.9 mol m^{-3} s^{-1} at 47 Pa of NO_2, 100 kPa of N_2, conditions that maintain kinetics in the low-pressure limit[38]) are similar to measured nitrate formation rates normalized to the pore volume of BaO/Al_2O_3 (0.38 mol m^{-3} s^{-1} at 47 Pa of NO_2), consistent with the kinetic relevance of the NO_2 dimerization reaction for nitrate formation on samples that contain high densities of $Ba(NO_2)_2$ sites.

Our kinetic data seem at odds with molecular beam studies in which NO_2 was dosed onto BaO/Al_2O_3 at 400−600 K.[13] Nitrate saturation occurs after ~10^3 s of NO_2 exposure at NO_2 fluxes equivalent to 10^{-3} Pa, but our kinetic data extrapolated to 10^{-3} Pa of NO_2 predict that nitrate saturation would require more than 10^{12} s. The high nitrate formation rates in the molecular beam study[13] may have resulted from the high N_2O_4 pressure in the source gas of the molecular beam (kept at 10 Pa of NO_2, 298 K), which could have led to a higher N_2O_4 concentration in the molecular beam than is in equilibrium with 10^{-3} Pa of NO_2 at 400−600 K.

The low equilibrium concentrations and slow formation rates of NO_2 dimers that are necessary to oxidize nitrites to more stable nitrates lead to low nitrate formation rates on BaO/Al_2O_3 at temperatures above 453 K. These slow NO_2 dimerization rates combined with unfavorable nitrite−carbonate thermodynamics (section 3.3) make BaO/Al_2O_3 adsorbents impractical at the high space velocities and low residual NO_2 levels in exhaust treatment systems. NO_x storage materials become practical only if alternate catalytic oxidation sites provide stronger oxidants than NO_2 at rates much larger than for homogeneous NO_2 dimerization pathways.

3.5. Kinetics of Nitrite and Nitrate Formation on $BaO/Pt/Al_2O_3$. Nitrite formation rates on BaO/Al_2O_3 and $BaO/Pt/Al_2O_3$ (at initial saturation carbonate coverages) were very similar during contact with NO/NO_2 mixtures (Table 1), indicating that the presence of Pt did not influence the rate of formation of nitrites. Nitrite formation rates were much higher than the rates at which nitrites were subsequently converted to nitrates on all materials (Table 1). Consequently, nitrites occupied most binding sites on BaO domains before detectable amounts of nitrate were formed during contact with NO/NO_2 mixtures (Figure 4).

Nitrate formation rates at saturation nitrite coverages were much higher on $BaO/Pt/Al_2O_3$ (coimpregnated with 0.0059 Pt clusters nm^{-2}, 3.0 BaO nm^{-2}) than on BaO/Al_2O_3 (3.0 BaO nm^{-2}) (Table 1). These data indicate that oxidants formed on Pt surfaces mediate nitrite conversion to nitrates faster than homogeneous NO_2 dimerization to N_2O_4, which limit nitrate formation rates on Pt-free samples. Pt sites apparently convert NO_2 to N_2O_4 or to an alternate oxidant (O atoms or other N_xO_y molecules) at much higher rates than homogeneous dimerization routes.

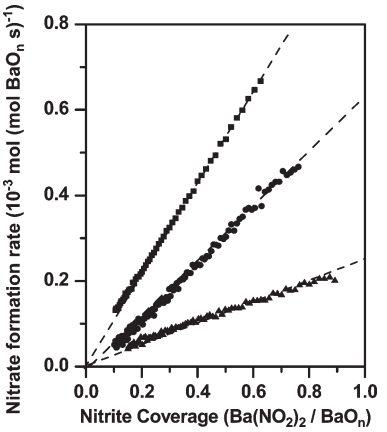

Figure 10. Nitrate formation rates normalized by BaO_n and plotted as a function of nitrite coverage on $BaO/Pt/Al_2O_3$ treated with a mixture of 5.2 Pa of NO_2 and 75 Pa of NO at (▲) 473 K, (●) 503 K, and (■) 523 K. Samples were treated with 100 Pa of NO_2 (0.5 h) and then 3 kPa of H_2 (0.5 h) before introduction of NO/NO_2 mixtures. The nitrite coverage evolved from high to low values for the reported data.

Nitrate formation rates on coimpregnated $BaO/Pt/Al_2O_3$ were much larger than on BaO/Al_2O_3 samples mixed with Pt/Al_2O_3 powders (3:1 ratio) by mechanical grinding (Table 1). These strong effects of the distance between Pt and BaO sites on nitrate formation rates suggest that the oxidant involved is unstable and present at very low concentrations and is therefore consumed near Pt sites that form this oxidant. Thus, Ba nitrite species are inaccessible to the oxidant unless Pt clusters are present within distances smaller than the micrometer dimensions of the physical mixtures.

Nitrites, however, were fully converted to nitrates on $BaO/Pt/Al_2O_3$ (Figure 4), suggesting that the distances between Pt and BaO sites in coimpregnated samples allow the oxidant to access all nitrite binding sites, not all of which are likely to reside within atomic distances of Pt clusters (present at 0.0059 Pt clusters nm^{-2}). Nitrate formation rates on $BaO/Pt/Al_2O_3$ decreased linearly with decreasing nitrite coverage as nitrites were converted to nitrates (Figure 10), suggesting that nitrate formation via Pt-mediated pathways is limited by irreversible reactions on BaO sites and that the oxidant is formed at equilibrium concentrations on Pt sites and is present at the same concentration throughout all nitrite structures on $BaO/Pt/Al_2O_3$. The uniform nitrite reactivity is inconsistent with the requirement for atomic contact between Pt and BaO sites, in view of the much higher density of

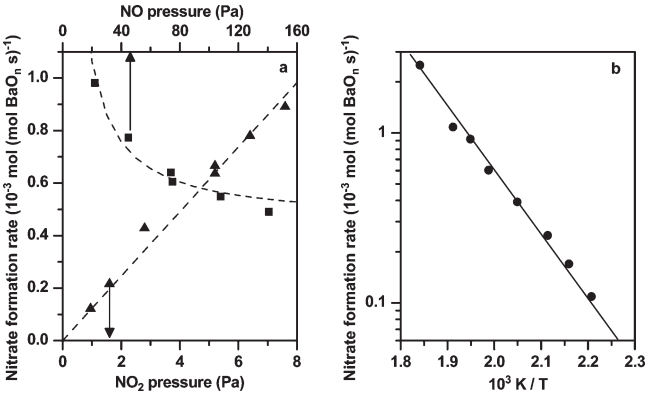

Figure 11. Nitrate formation rates normalized by BaO_n and extrapolated to saturation nitrite coverage on $BaO/Pt/Al_2O_3$. (a) Rates at 503 K versus (▲) NO_2 (at 75 Pa of NO) and (■) NO (at 5.2 Pa of NO_2) pressures and (b) at 75 Pa of NO and 5.2 Pa of NO_2 as a function of temperature plotted in an Arrhenius format. $BaO/Pt/Al_2O_3$ was treated with 100 Pa of NO_2 (0.5 h) and then 3 kPa of H_2 (0.5 h) before each measurement. The dashed curves show predictions of eq 10.

BaO_n sites (0.75 BaO nm^{-2}) than Pt clusters (0.0059 Pt clusters nm^{-2}). The linear decrease in rates with nitrite conversion also shows that the formation rates and the mobility of the oxidant species are much faster that the adsorption rates (more detailed arguments are provided in the Supporting Information, section S.1). This conclusion, taken together with lack of atomic contact between Pt and BaO, renders any claims for atomic oxygen as the Pt-generated oxidant implausible. We conclude that reactions on Pt establish an equilibrium between the NO_2 and NO reactants and the reactive oxidant species and that the latter diffuse rapidly among Pt and BaO sites to provide uniform oxidant concentrations throughout $BaO/Pt/Al_2O_3$ samples.

Our mechanistic proposal contrasts with previous kinetic models that proposed two types of BaO sites, distinguished by their proximity to Pt clusters.[39−42] The linear dependence of nitrate formation rates on nitrite coverage (Figure 10) suggests instead that the proximity of BaO sites to Pt clusters is inconsequential to the rate of nitrate formation and that all sites are kinetically identical. These two-site models were based on rate data that required two kinetic parameters to describe the results.[39−42] The need for two kinetic parameters may have been related to the sequential formation of nitrites by NO/NO_2 coadsorption and then nitrates by NO_2 reactions with nitrites or to the formation of nitrates on BaO and on Al(O)OH sites, which was not considered in these previous kinetic descriptions.

The kinetics of nitrate formation via Pt-mediated routes on $BaO/Pt/Al_2O_3$ and in particular the linear decrease in rates with increasing extents of nitrite conversion (Figure 10) differ markedly from nitrite formation dynamics mediated by homogeneous NO_2 dimerization on BaO/Al_2O_3 (eq 6). Nitrate formation rates on $BaO/Pt/Al_2O_3$ (extrapolated to the initial saturated nitrite coverages) increased linearly with NO_2 pressure (Figure 11a); rates were inhibited by NO (Figure 11a) and were sensitive to temperature (453−540 K) with an apparent activation energy of 68 ± 5 kJ mol^{-1} (Figure 11b). Nitrate formation rates ($r_{n\text{-}N,Pt}$) on $BaO/Pt/Al_2O_3$ were accurately described by the empirical rate equation

$$r_{n-N,Pt} = k_{n-N,Pt}[NO_2]^{0.94}[NO]^{-0.38}[Ba(NO_2)_2]^{1.0} \quad (8)$$

Scheme 2. Plausible Elementary Steps for the Conversion of Nitrites to Nitrates on $BaO/Pt/Al_2O_3$

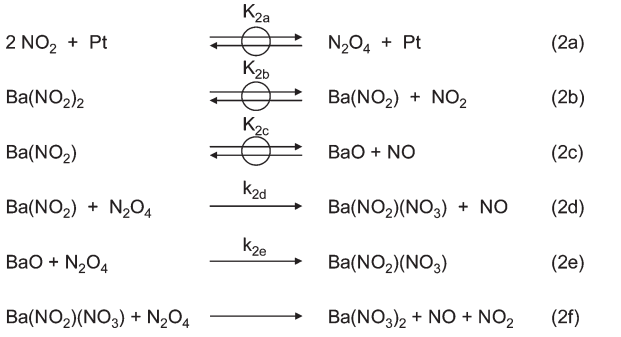

the functional form of which cannot be rigorously reconciled with any sequence of elementary steps.

The different nitrate formation rate equations of $BaO/Pt/Al_2O_3$ (eq 8) and BaO/Al_2O_3 (eq 6) reflect corresponding differences in the kinetically relevant steps that form or consume the oxidants required to convert nitrites to nitrates. Nitrate formation rates via homogeneous pathways increased with $(NO_2)^2$ and were independent of coverage (eq 6) or temperature, consistent with nitrite oxidation steps that involve kinetically relevant NO_2 dimerization instead of direct NO_2 reactions with nitrites. In contrast, rates via Pt-mediated routes were proportional to NO_2 pressure and to residual $Ba(NO_2)_2$ concentrations and inhibited by NO (eq 8). Pt is unlikely to facilitate direct reactions between nitrite and O atoms or NO_2, because all BaO sites cannot plausibly be located in atomic proximity to a Pt cluster yet still convert nitrites to nitrates with uniform rates. Therefore, the effects of NO and NO_2 pressures on nitrate formation rates on $BaO/Pt/Al_2O_3$ must reflect the formation of equilibrium concentrations of the relevant oxidant on Pt sites and the kinetic consequences of these oxidant concentrations on nitrite conversion to nitrates.

N_2O_4 intermediates are involved in nitrate formation via homogeneous pathways (section 3.4) and are plausible as nitrite oxidants formed on Pt sites. The thermodynamics of NO_3, an alternate strong oxidant, are known,[24] but equilibrium NO_3 pressures (4×10^{-12} Pa) are much smaller than for N_2O_4 (9×10^{-8} Pa) under the conditions of these experiments (4 Pa of NO_2, 70 Pa of NO, 503 K); therefore, we consider NO_3 a less plausible oxygen atom carrier than N_2O_4. Scheme 2 shows a sequence of elementary steps for nitrite oxidation to nitrate mediated by N_2O_4 species formed by equilibrated reactions on Pt (step 2a). Equilibrium N_2O_4 concentrations are proportional to $[NO_2]^2$, but the observed nitrate formation rates are first-order in NO_2 (eq 8). This suggests that NO_2 desorbs from a $Ba(NO_2)_2$ site in a quasi-equilibrated step (step 2b) to form a reactive intermediate $[Ba(NO_2)]$ on which N_2O_4 adsorbs (step 2d); the concentration of this $Ba(NO_2)$ intermediate is proportional to $[NO_2]^{-1}$ on surfaces saturated by $Ba(NO_2)_2$. The NO inhibition evident from eq 8 suggests that NO desorption from $Ba(NO_2)$ (step 2c) also occurs before N_2O_4 adsorbs (step 2e). A final elementary step is required to convert $Ba(NO_2)(NO_3)$, the product of N_2O_4 adsorption on BaO or $Ba(NO_2)$ sites, to $Ba(NO_3)_2$ (step 2f). The assumptions of irreversible N_2O_4 adsorption (by steps 2d and 2e) and of $Ba(NO_2)_2$ and $Ba(NO_3)_2$

as most abundant surface species give nitrate formation rates ($r_{n\text{-}N,Pt}$) as

$$r_{n-N,Pt} = (K_{2a}[NO_2]^2)\frac{(k_{2d} + k_{2e}K_{2c}[NO]^{-1})}{K_{2b}{}^{-1}[NO_2]}[Ba(NO_2)_2] \quad (9)$$

$$r_{n-N,Pt} = \lambda[NO_2](1 + \mu[NO]^{-1})[Ba(NO_2)_2] \quad (10)$$

where λ represents $K_{2a}K_{2b}k_{2d}$ and μ represents $K_{2c}(k_{2d})^{-1}k_{2e}$. Equation 10 accurately predicts the first-order NO_2 and $Ba(NO_2)_2$ dependences and NO inhibition of measured nitrate formation rates (dashed curves in Figures 10 and 11a). The apparent activation energy (68 kJ mol^{-1}) appears to reflect a combination of the exothermic formation of N_2O_4 (−57 kJ mol^{-1},[24] represented in K_{2a}) and the endothermic desorption of NO_2 or NO from $Ba(NO_2)_2$ surfaces [147 kJ mol^{-1} on BaO(100)[36] for each of NO_2 and NO, represented in K_{2b} and K_{2c}].

These results provide evidence for the synergistic roles of Pt oxidation catalysts and BaO adsorbents in lean de-NO_x trapping strategies. Pt is necessary to catalyze NO oxidation to more reactive NO_2 molecules, but NO_2 inhibits NO oxidation;[6,7] therefore, BaO sites must rapidly and irreversibly bind NO_2 to lower its concentration and increase NO oxidation rates.[7] NO_2 adsorption on BaO-containing solids in streams containing high CO_2 concentrations requires storage as stable nitrates that are formed by reactions involving N_2O_4 oxidants. These N_2O_4 oxidants are formed much faster by reactions of NO_2 on Pt surfaces than by homogeneous NO_2 dimerization reactions. The low stability and low equilibrium concentrations of N_2O_4 intermediates, however, imply that Pt and BaO sites must be present in nanometer-scale distances to increase nitrate formation rates over levels achieved by homogeneous pathways; therefore, the coimpregnation of metal and basic oxide substrates is required to realize the synergistic effects that allow efficient NO_x storage on catalyst-adsorbent materials.

4. CONCLUSIONS

NO and NO_2 adsorb on BaO/Al_2O_3 and $BaO/Pt/Al_2O_3$ to initially form nitrites that are subsequently oxidized to nitrates by NO_2-derived intermediates. Nitrites are formed by a nonactivated process when NO and NO_2 bind molecularly at vicinal positions on BaO surfaces. Nitrites readily displace preformed surface carbonates when CO_2 is absent from reactant streams, but the addition of CO_2 to NO/NO_2 mixtures decreases steady-state nitrite coverages because of competitive binding between CO_2 as carbonate and NO/NO_2 as nitrite. A majority of BaO binding sites behave as a uniform ensemble for nitrite−carbonate interconversion reactions, with an equilibrium constant that leads to low nitrite coverages at CO_2/NO_x levels present in combustion exhaust. Nitrates are more stable than nitrites, but the oxidation of nitrites to nitrates on BaO/Al_2O_3 occurs slowly and requires an oxidant in the form of N_2O_4 that is produced by nonactivated bimolecular collisions of NO_2 molecules in the gas phase. Nitrate formation becomes much faster when Pt sites are present in close (but not atomic) proximity to Ba nitrite sites, because reactions on Pt sites establish equilibrium concentrations of N_2O_4 oxidants that react subsequently with nitrites on BaO surfaces.

APPENDIX: DETERMINATION OF ADSORBATE COVERAGES

Adsorbate coverages on BaO/Al_2O_3 were determined from infrared spectra by assuming that coverages ($\boldsymbol{\theta}$) and spectra ($\mathbf{Z}$) are related by response factors ($\mathbf{F}$):

$$\mathbf{Z} = \boldsymbol{\theta}\mathbf{F} \quad (A.1)$$

Here, $\boldsymbol{\theta}$ and $\mathbf{Z}$ are treated as matrices with each row of $\mathbf{Z}$ corresponding to an infrared spectrum and each row of $\boldsymbol{\theta}$ corresponding to the coverage of all adsorbates during an infrared measurement. The response factors ($\mathbf{F}$) can also be treated as a matrix when they are independent of coverage, which leads to coverages described by

$$\boldsymbol{\theta} = \boldsymbol{\theta}(\mathbf{F}\mathbf{F}^T)(\mathbf{F}\mathbf{F}^T)^{-1} = \mathbf{Z}\mathbf{F}^T(\mathbf{F}\mathbf{F}^T)^{-1} \quad (A.2)$$

Equation A.2 involves matrix transpose, inverse, and multiplication operations.

The adsorbate coverages reported in this study were computed from eq A.2, using response factors derived from matrix representations of the spectra in Figures 1 or 2. The response factors were normalized to reflect measured CO_2, NO, and NO_2 uptakes on BaO/Al_2O_3. Similar response factors were assumed for BaO/Al_2O_3 and for $BaO/Pt/Al_2O_3$, and variation in the wafer thickness was corrected by comparing the carbonate bands with the CO_2 uptake.

The assumption that the response factors are independent of coverage can be assessed from the effects of coverage on infrared bandwidths and band centers or analyzed statistically by factor analysis,[43] which considers spectral features, $\mathbf{E}$, that are not explained by the chosen response factors

$$\mathbf{E} = \mathbf{Z} - \boldsymbol{\theta}\mathbf{F} \quad (A.3)$$

The spectral features that were unexplained by the deconvolution procedure that led to Figure 3a are shown in the Supporting Information (Figure S1). The sum of squares of the unexplained data was much less than the sum of squares of the explained data (their ratio was 2×10^{-5}), and no spectrally significant features were observed in the unexplained data.

ASSOCIATED CONTENT

Supporting Information. Figure S1 (spectral residuals resulting from deconvolution of infrared spectra), Figure S2 (carbonate, nitrite, and nitrate uptakes versus temperature), Figure S3 (carbonate and nitrite coverage versus CO_2, NO, and NO_2 pressures), Figure S4 (quilibrium nitrite coverages at constant values of ψ ($[NO][NO_2][CO_2]^{-1}$), and section S.1 (effect of diffusion on reactive intermediate concentration). This material is available free of charge via the Internet at http://pubs.acs.org.

AUTHOR INFORMATION

Corresponding Author
*E-mail: iglesia@cchem.berkeley.edu.

ACKNOWLEDGMENT

We acknowledge financial support from The Ford Motor Co., General Motors, the Chevron Corp.; and the Chemical Sciences, Geosciences, Biosciences Division, Office of Basic Energy

Sciences, Office of Science US Department of Energy (Grant Number DE-FG02-03ER15479). We are also grateful to Profs. Johannes Lercher (Technical University-Munich) and Raul Lobo (University of Delaware) for helpful technical discussions and insights. We thank Mr. Rajamani Gounder for carefully proofreading the manuscript.

REFERENCES

(1) Takahashi, N.; Shinjoh, H.; Iijima, T.; Suzuki, T.; Yamazaki, K.; Yokoto, K.; Suzuki, H.; Miyoshi, N.; Matsumoto, S.; Tanizawa, T.; Tanaka, T.; Tateishi, S.; Kasahara, K. *Catal. Today* **1996**, *27*, 63.
(2) Epling, W. S.; Campbell, L. E.; Yezerets, A.; Currier, N. W.; Parks, J. E. *Catal. Rev.: Sci. Eng.* **2004**, *46*, 163.
(3) Roy, S.; Baiker, A. *Chem. Rev.* **2009**, *109*, 4054.
(4) Cant, N. W. *Catal. Today* **2002**, *73*, 271.
(5) Fridell, E.; Persson, H.; Westerberg, B.; Olsson, L.; Skoglundh, M. *Catal. Lett.* **2000**, *66*, 71.
(6) Mulla, S. S.; Chen, N.; Delgass, W. N.; Epling, W. S.; Ribeiro, F. H. *Catal. Lett.* **2005**, *100*, 267.
(7) Weiss, B. M.; Iglesia, E. *J. Phys. Chem. C* **2009**, *113*, 13331.
(8) Weiss, B. M.; Iglesia, E. *J. Catal.* **2010**, *272*, 74.
(9) Sedlmair, C.; Seshan, K.; Jentys, A.; Lercher, J. A. *J. Catal.* **2003**, *213*, 308.
(10) Schmitz, P. J.; Baird, R. J. *J. Phys. Chem. B* **2002**, *106*, 4172.
(11) Ji, Y.; Toops, T. J.; Pihl, J. A.; Crocker, M. *Appl. Catal. B: Environ.* **2009**, *91*, 329.
(12) Desikusumastuti, A.; Happel, M.; Dumbuya, K.; Staudt, T.; Laurin, M.; Gottfried, J. M.; Steinruck, H. P.; Libuda, J. *J. Phys. Chem. C* **2008**, *112*, 6477.
(13) Desikusumastuti, A.; Staudt, T.; Happel, M.; Laurin, M.; Libuda, J. *J. Catal.* **2008**, *260*, 315.
(14) Yi, C. W.; Szanyi, J. *J. Phys. Chem. C* **2009**, *113*, 716.
(15) Frola, F.; Prinetto, F.; Ghiotti, G.; Castoldi, L.; Nova, I.; Lietti, L.; Forzatti, P. *Catal. Today* **2007**, *126*, 81.
(16) Forzatti, P.; Castoldi, L.; Nova, I.; Lietti, L.; Tronconi, E. *Catal. Today* **2006**, *117*, 316.
(17) Yi, C. W.; Kwak, J. H.; Szanyi, J. *J. Phys. Chem. C* **2007**, *111*, 15299.
(18) Hess, C.; Lunsford, J. H. *J. Phys. Chem. B* **2002**, *106*, 6358.
(19) Kabin, K. S.; Khanna, P.; Muncrief, R. L.; Medhekar, V.; Harold, M. P. *Catal. Today* **2006**, *114*, 72.
(20) Mazhoul, H.; Brilhac, J. F.; Gilot, P. *Appl. Catal. B: Environ.* **1999**, *20*, 47.
(21) Cant, N. W.; Liu, I. O. Y.; Patterson, M. J. *J. Catal.* **2006**, *243*, 309.
(22) Desikusumastuti, A.; Staudt, T.; Qin, Z.; Happel, M.; Laurin, M.; Lykhach, Y.; Shaikutdinov, S.; Rohr, F.; Libuda, J. *ChemPhysChem* **2008**, *9*, 2191.
(23) Piacentini, M.; Maciejewski, M.; Baiker, A. *Appl. Catal. B: Environ.* **2005**, *59*, 187.
(24) *CRC Handbook of Chemistry and Physics*, 91st ed.; Haynes, W. M., Ed.; CRC Press/Taylor and Francis: Boca Raton, FL, 2011.
(25) Mirth, G.; Eder, F.; Lercher, J. A. *Appl. Spectrosc.* **1994**, *48*, 194.
(26) Koros, R. M.; Nowak, E. J. *Chem. Eng. Sci.* **1967**, *22*, 470.
(27) Busca, G.; Lorenzelli, V. *Mater. Chem.* **1982**, *7*, 89.
(28) Epling, W. S.; Peden, C. H. F.; Szanyi, J. *J. Phys. Chem. C* **2008**, *112*, 10952.
(29) Frola, F.; Manzoli, M.; Prinetto, F.; Ghiotti, G.; Castoldi, L.; Lietti, L. *J. Phys. Chem. C* **2008**, *112*, 12869.
(30) Wood, D. L. *J. Chem. Phys.* **1981**, *75*, 4809.
(31) Hadjiivanov, K. I. *Catal. Rev.: Sci. Eng.* **2000**, *41*, 71.
(32) Desikusumastuti, A.; Staudt, T.; Gronbeck, H.; Libuda, J. *J. Catal.* **2008**, *255*, 127.
(33) Nova, I.; Castoldi, L.; Lietti, L.; Tronconi, E.; Forzatti, P.; Prinetto, F.; Ghiotti, G. *J. Catal.* **2004**, *222*, 377.
(34) Knozinger, H. *Adv. Catal.* **1976**, *25*, 184.
(35) Cant, N. W.; Liu, I. O. Y.; Patterson, M. J. *Appl. Catal. B: Environ.* **2007**, *77*, 12.
(36) Schneider, W. F. *J. Phys. Chem. B* **2004**, *108*, 273.
(37) Butt, J. B. *Reaction Kinetics and Reactor Design*; Marcel Dekker, Inc.: New York, 2000.
(38) Borrell, P.; Cobos, C. J.; Luther, K. *J. Phys. Chem.* **1988**, *92*, 4377.
(39) Bhatia, D.; Clayton, R. D.; Harold, M. P.; Balakotaiah, V. *Catal. Today* **2009**, *147S*, S250.
(40) Kromer, B. R.; Cao, L.; Cumaranatunge, L.; Mulla, S. S.; Ratts, J. L.; Yezerets, A.; Currier, N. W.; Ribeiro, F. H.; Delgass, W. N.; Caruthers, J. M. *Catal. Today* **2008**, *136*, 93.
(41) Epling, W. S.; Parks, J. E.; Campbell, G. C.; Yezerets, A.; Currier, N. W.; Campbell, L. E. *Catal. Today* **2004**, *96*, 21.
(42) Forzatti, P.; Castoldi, L.; Nova, I.; Lietti, L.; Tronconi, E. *Catal. Today* **2006**, *117*, 316.
(43) Malinowski, E. R. *Factor Analysis in Chemistry*; John Wiley and Sons: New York, 1991.